Eur. Phys. J. B **60**, 203–215 (2007)
DOI: 10.1140/epjb/e2007-00333-x

THE EUROPEAN PHYSICAL JOURNAL B

# A data-analysis method for identifying differential effects of time-delayed feedback forces and periodic driving forces in stochastic systems

A. Wilmer[1], T.D. Frank[1,2,a] P.J. Beek[3], and R. Friedrich[1]

[1] Institute for Theoretical Physics, University of Münster, Wilhelm-Klemm-Str. 9, 48149 Münster, Germany
[2] Center for the Ecological Study of Perception and Action, University of Connecticut, 406 Babbidge Road, Storrs, CT 06269, USA
[3] Faculty of Human Movement Sciences and Research Institute Move, VU University Amsterdam, Van der Boechorststraat 9, 1081 BT Amsterdam, The Netherlands

Received 25 March 2007
Published online 8 December 2007 – 

**Abstract.** In this work a method is developed for analyzing time series of periodically driven stochastic systems involving time-delayed feedback. The proposed data-analysis method yields dynamical models in terms of stochastic delay differential equations. On the basis of these dynamical models differential effects of driving forces and time-delayed feedback forces can be identified.

**PACS.** 02.30.Ks Delay and functional equations – 05.45.Tp Time series analysis – 87.19.St Movement and locomotion

## 1 Introduction

An important task in modern physics is the understanding and modeling of complex systems that operate far from thermal equilibrium. However, a microscopic bottom-up description of such systems is mathematically unfeasible because complex nonequilibrium systems typically exhibit a huge number of degree of freedoms. In contrast, a macroscopic top-down description in terms of order parameter equations can often be obtained [1–4]. In general, complex systems exhibit fluctuations because the internal processes that govern their functioning are intrinsically noisy and because they are in contact with their environments. Therefore, order parameter equations often assume the form of stochastic differential equations such as Langevin equations.

In this study, we will exploit this level of description of stochastic differential equations in order to study periodically forced feedback control systems that exhibit fluctuations. Such systems involve both periodic driving forces and time-delayed feedback loops in addition to noise sources that give rise to fluctuations. Periodic driving forces occur in various systems like seasonally driven biological systems and periodically driven systems in physics, biology, and engineering sciences. Periodically forced feedback control systems form an important subclass of such systems. In such a system the feedback control tends to establish a particular desired relationship between the system output and the driving force. Stochastic feedback systems that are periodically driven have been discussed frequently in the literature (e.g. in the context of linear response theory [5], stochastic resonance [6], and periodically forced thermal ratchet models for Brownian motors [7–13]). However, feedback loops involve time-delays. Such time-delayed feedback systems have been discussed in biology [14–24], physics [25–36], and engineering applications [37–43]. In general, they are described by delayed ordinary differential equations and exhibit a variety of interesting phenomena such as delay-induced bifurcations of fixed points to oscillatory and chaotic solutions [15, 16,25,28], delay-induced resonances and re-entrant bifurcations [44], and delay-induced non-invasive stabilization processes [27]. However, in most studies on driven noisy feedback systems these time-delays have been neglected (for an exception see e.g. [45]). In particular, from the viewpoint of time series analysis [46,47] the question arises how to identify the impacts of the periodic driving forces and of time-delayed feedback loops on the basis of time series data.

For example, in order to gain insight into the mechanisms underlying coordinated motor behavior it is most

[a] e-mail: tdfrank@uni-muenster.de

helpful to study rhythmic limb movements that are paced by a metronome beat or synchronized with an oscillating target [48–55]. In such experimental setups, the actually performed movement patterns arise again from an interplay of a periodic driving force (the metronome beat or oscillating target) and a control process that involves a time delay in terms of a neurophysiological signal transmission delay or a reaction time delay. Likewise, we may think of the engineering problem to construct anti-roll devices for ships. In general, ship rolling arises from periodically emerging water waves. This rolling motion is usually suppressed by means of a time-delayed control mechanism that involves fin movements or the loading and unloading of anti-roll water tanks [56,57]. The still remaining (small amplitude) rolling motions of the ship result from the interplay of a periodic driving force (i.e. the water waves) and a time-delayed control mechanism (i.e. the anti-roll device). Finally, studies on forced thermal ratchet models showed that propagation of Brownian motors is probably due to the interplay between periodically time-dependent driving forces, spatially periodic, asymmetric potential forces, and thermal fluctuating forces [7–13].

In principle, time series analysis could make an essential contribution in studying how periodic driving forces and time-delayed control processes may interact with each other. However, to this end, a data-analysis method needs to be developed that is able to distinguish between the effects of these two qualitatively different processes. Moreover, the data-analysis method in question needs to be able to deal with noisy data.

In Section 2 we will propose a data-analysis method which satisfies these needs. The proposed data-analysis method applies to a broad class of drift-diffusion processes that will be defined in Section 2.1. In several earlier studies it has been shown how to estimate the coefficients of similar drift-diffusion processes from noisy data [58–66]. In particular, it has been shown how to derive the relevant drift and diffusion coefficients for periodically driven noisy systems [67] and for noisy systems involving time-delayed feedback loops [68], see Figure 1. Moreover, several data-analysis techniques for time-delayed deterministic systems have been proposed (see [69–71] and references therein). In Section 2.2 we will show how to determine these coefficients for noisy systems that involve both a periodic driving force and a time-delayed feedback force. That is, the missing link (see Fig. 1) between the analysis of periodically driven and time-delayed systems will be established. In Section 2.3 a self-consistency test based on first-order statistical properties will be discussed. The purpose of this self-consistency test is to show whether or not the a priori hypothesis is correct at all that a given process belongs to the aforementioned class of drift-diffusion processes.

In Section 3 we will illustrate the data-analysis method by means of some examples. Examples of first-order dynamical systems will be presented in Section 3.1. An example of a second-order dynamical system that has been proposed to describe paced tapping will be discussed in Section 3.2.

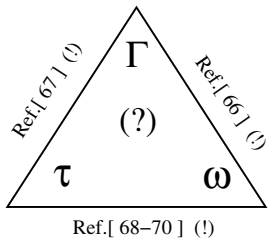


**Fig. 1.** Solved (!) and unsolved (?) problems. The symbols $\Gamma$, $\omega$, $\tau$ represent different kinds of systems. $\Gamma$: noisy systems. $\omega$ periodically driven systems. $\tau$ time-delayed system. A data-analysis method that is dealing with $\Gamma$ and $\omega$ has been proposed in [67]. A method that is dealing with $\Gamma$ and $\tau$ has been developed in [68]. The case $\Gamma$, $\omega$, and $\tau$ is discussed in the present study.

## 2 Method

### 2.1 Drift-diffusion processes

In this study we consider stochastic processes that satisfy non-autonomous stochastic delay differential equations of first or higher order. For the sake of clarity we will demonstrate the details of the proposed technique for first-order dynamical systems. Accordingly, we assume that we are dealing with noisy periodically-driven time-delayed systems that can be described by a univariate stochastic delay differential equation of the form

$$\frac{\mathrm{d}}{\mathrm{d}t}X = h\left(X, Y, F(t)\right) + g\left(X, Y, F(t)\right)\Gamma(t). \qquad (1)$$

Here, $X(t)$ denotes a random variable that describes the state of the system. $Y(t)$ is the corresponding time-delayed (or retarded) state variable. That is, we have $Y(t) = X(t-\tau)$, where $\tau$ denotes the time delay. The function $F(t)$ describes a periodic driving force with period $T$ (i.e. we have $F(t) = F(t+T)$). In equation (1) the drift function $h$ describes the deterministic evolution of the state variable. The term $g\Gamma$ describes a fluctuating force or a noise source with $g$ corresponding to the noise amplitude. The function $\Gamma(t)$ is the Langevin force [5] with $\langle\Gamma(t)\rangle = 0$ and $\langle\Gamma(t)\Gamma(t')\rangle = 2\delta(t-t')$, where $\delta(\cdot)$ denotes the Dirac delta function and $\langle\cdot\rangle$ represents an ensemble average. Note that in order to interpret the product $g\Gamma$ we will use the Itô-interpretation for stochastic integrals [72] which applies also to time-delayed systems [73,74].

Equation (1) can be regarded as a time-delayed Langevin equation. In particular, if $h$ and $g$ do not depend on the retarded variable $Y$, then equation (1) reduces to an ordinary Langevin equation. In general, Langevin equations describe continuous but non-differentiable processes [5] such that strictly speaking the differential quotient $\mathrm{d}X/\mathrm{d}t$ is not well-defined. In order to avoid the notation $\mathrm{d}X/\mathrm{d}t$, one may cast equation (1) into the form $\mathrm{d}X = h\mathrm{d}t + g\mathrm{d}B$, where $B$ is a Wiener process with variance proportional to $\mathrm{d}t$. Nevertheless, in our study and in line with a comprehensive part of the literature on stochastic processes, we will use the notation $\mathrm{d}X/\mathrm{d}t$ that nicely indicates that equation (1) is an evolution equation.

In order to obtain a complete description of a delay system as defined by equation (1) we need to specify the initial condition $x(t)$ for $t \in [-\tau, 0]$. The fact that the initial condition corresponds to a function and not to a finite set of parameters indicates that the phase space of the dynamics defined by equation (1) is not one-dimensional but infinitely large. For example, replacing $x(t-\tau)$ by $\exp\{-\tau \mathrm{d}/\mathrm{d}t\}x(t)$ and truncating the Taylor series of the exponential function after $p$ terms, we realize that equation (1) corresponds to a $p$-dimensional system with $p$ initial conditions in the limit $p \to \infty$.

Being aware of the abovementioned difficulties concerning the differentiability and the initial conditions of the stochastic processes under consideration, we can now proceed and simplify the notation of equation (1) even further. Accordingly, we write equation (1) as

$$\frac{\mathrm{d}}{\mathrm{d}t}X = h\left(X, Y, t\right) + g\left(X, Y, t\right) \Gamma(t). \tag{2}$$

The conditional probability density $P(x,t|x',t';y,t-\tau) = \langle \delta(x - X(t)) \rangle|_{x'=X(t'),y=X(t-\tau)}$ satisfies a delay Fokker-Planck equation of the form [74]

$$\frac{\partial}{\partial t} P(x,t|x',t';y,t-\tau) = \hat{L}\, P(x,t|x',t';y,t-\tau) \tag{3}$$

with the Fokker-Planck operator

$$\hat{L} = -\frac{\partial}{\partial x} h(x,y,t) + \frac{\partial^2}{\partial x^2} D(x,y,t) \tag{4}$$

and $D(x,y,t) = g^2(x,y,t)$. The coefficient $D$ will be referred to as diffusion coefficient.

## 2.2 Drift-diffusion estimation

### 2.2.1 Basics

Following [74], we can show that the relations

$$h(x,y,t) = \lim_{\epsilon \to 0} \frac{1}{\epsilon} \langle X(t+\epsilon) - x \rangle \Big|_{X(t)=x, X(t-\tau)=y}, \tag{5}$$

$$D(x,y,t) = \lim_{\epsilon \to 0} \frac{1}{2\epsilon} \left\langle \left(X(t+\epsilon) - x\right)^2 \right\rangle \Big|_{X(t)=x, X(t-\tau)=y}. \tag{6}$$

hold. In general, the conditional averages in equations (5) and (6) have to be computed from ensembles of trajectories $X(t)$. However, we would like to exploit the periodicity of the problem at hand and evaluate time averages instead of ensemble averages. Therefore, we will discuss next how the ensemble averages can be replaced by appropriately defined time averages.

### 2.2.2 Implementation for periodic driving forces

In order to simplify equations (5) and (6) we assume that we are dealing with a periodic process ([75], Chap. 5) with period $T$. That is, all (first- and higher-order) statistical quantities become invariant against time shifts of period $T$. As shown in [67] the ensemble averages in equations (7) and (8) can then be replaced by stroboscopic time averages such that we obtain

$$h(x,y,t_k) = \lim_{\epsilon \to 0} \frac{1}{\epsilon} \langle X(t_k+\epsilon) - x \rangle \Big|_{X(t_k)=x, X(t_k-\tau)=y}, \tag{7}$$

$$D(x,y,t_k) = \lim_{\epsilon \to 0} \frac{1}{2\epsilon} \left\langle \left(X(t_k+\epsilon) - x\right)^2 \right\rangle \Big|_{X(t_k)=x, X(t_k-\tau)=y}. \tag{8}$$

The variable $t_k \in T$ describes a particular time point in the period $T$ or a particular phase with respect to the periodic driver. Let $T^{(1)}$, $T^{(2)}$, $T^{(3)}$ and so on denote subsequent intervals of length $T$. Stroboscopic time averaging means that we average across these intervals $T^{(i)}$ for every fixed time point $t_k$.

### 2.2.3 Numerical implementation

In order to implement equations (7) and (8) on a computer, we introduce the three dimensional phase space $\Omega$ which is spanned by the state variable $x$, the time-delayed state variable $y$, and the periodic time coordinate $t$ mod $T$. That is, a point in $\Omega$ is described by the vector $\mathbf{q} = (x, y, t \bmod T)$. The drift and diffusion coefficients given by equations (7) and (8) are functions defined on this phase space $\Omega$.

First of all, one has to discretize $\Omega$ into bins. The binning was realized with equidistant intervals for $\Delta x$, $\Delta y$, and $\Delta t$, so that a volume element is given by

$$\Delta\Omega_{ijk} = \left([x_i, x_i + \Delta x), [y_j, y_j + \Delta y), [t_k, t_k + \Delta t)\right). \tag{9}$$

In addition, we use finite boundaries for $x$ and $y$ (i.e., we evaluate $x$ and $y$ only in a bounded domain $x, y \in [x_{\min}, x_{\max}]$). In doing so, $\Omega$ is discretized into a finite number of volume elements $\Delta\Omega$. We further introduce the indicator function $\chi$

$$\chi_{ijk}(\mathbf{q}) = \begin{cases} 1, & \mathbf{q} \in \Delta\Omega_{ijk}, \\ 0, & \text{otherwise.} \end{cases} \tag{10}$$

With the help of the indicator-function (10) one can formulate a discretized approximation for drift and diffusion:

$$h(x,y,t) = \sum_{ijk} h_{ijk}\, \chi_{ijk}(\mathbf{q}) + O(\Delta x, \Delta t), \tag{11}$$

$$D(x,y,t) = \sum_{ijk} D_{ijk}\, \chi_{ijk}(\mathbf{q}) + O(\Delta x, \Delta t). \tag{12}$$

Next, we implement the conditional averages occurring in equations (7) and (8) into a numerical algorithm over a

finite time series. To this end, we consider data recorded with a constant sampling time $\delta t$ (or sampling frequency $f = 1/\delta t$) at time points $t_n = n\delta t$ with $n = 1, \ldots, N$. Accordingly, we discretize the delay like $\tau = m\delta t$. As a result, we obtain for every data sample $n$ a vector $\mathbf{q}_n = (X_n, X_{n-m}, t_n \bmod T)$ with $X(t_n) = X_n$ and $X(t_n - \tau) = X_{n-m}$. The coefficients $h_{ijk}$ and $D_{ijk}$ can then be estimated from $h_{ijk} = \tilde{h}_{ijk} + O(\delta t, N^{-1/2})$, $D_{ijk} = \tilde{D}_{ijk} + O(\delta t, N^{-1/2})$ and

$$\tilde{h}_{ijk} = \frac{1}{\delta t} \frac{\sum_{n=0}^{N-1} (X_{n+1} - X_n)\, \chi_{ijk}(\mathbf{q}_n)}{\sum_{n=0}^{N-1} \chi_{ijk}(\mathbf{q}_n)}, \tag{13}$$

$$\tilde{D}_{ijk} = \frac{1}{2\delta t} \frac{\sum_{n=0}^{N-1} (X_{n+1} - X_n)^2\, \chi_{ijk}(\mathbf{q}_n)}{\sum_{n=0}^{N-1} \chi_{ijk}(\mathbf{q}_n)}. \tag{14}$$

The error terms of order $\delta t$ and $1/\sqrt{N}$ vanish in the limits $\delta t \to 0$ and $N \to \infty$. Combining equations (11), (12) and equations (13), (14), we obtain a numerical implementation of equations (7) and (8) given by

$$h(x, y, t) = \sum_{ijk} \tilde{h}_{ijk}\, \chi_{ijk}(\mathbf{q}) + O(\Delta x, \Delta t, \delta t, N^{-\frac{1}{2}}), \tag{15}$$

$$D(x, y, t) = \sum_{ijk} \tilde{D}_{ijk}\, \chi_{ijk}(\mathbf{q}) + O(\Delta x, \Delta t, \delta t, N^{-\frac{1}{2}}). \tag{16}$$

Further discussions on the error terms can be found in [76–79]. Measurement errors are also discussed in [80,81].

### 2.3 Test of self-consistency

In order to test our a priori hypothesis that a given time series can be reproduced from a drift-diffusion model of the form (1) we compare statistical quantities of the original time series with those computed from the corresponding drift-diffusion model (1). In what follows we will consider only first-order statistical quantities. For tests involving higher-order statistical quantities the reader is referred to [58,82].

A general first-order statistical quantity of a stochastic process is the probability density of that process. All moments and expectation values can be computed from that density measure. For periodically driven systems that exhibit time-periodic stochastic processes the probability density is a periodic function of time (see Sect. 2.2.2). Therefore, in the present context of periodically driven systems it is useful to compare time-periodic probability densities computed from original data with time-periodic probability densities computed from the drift-diffusion models (1) derived from the original data. To this end, however, we need to re-normalize probability densities with respect to the domain $[r_{\min}, r_{\max}]$ on which reliable estimates for the drift and diffusion coefficients of the stochastic models are available[1]. For example, let $P_{\text{org}}(x,t)$ with $P_{\text{org}}(x,t) = P_{\text{org}}(x, t+T)$ denote the time-periodic probability density computed from an original data set involving a state variable $x$ defined on the real number line. Let $P_{\text{rec}}(x,t)$ with $P_{\text{rec}}(x,t) = P_{\text{rec}}(x, t+T)$ denote the probability density computed from a drift-diffusion model (1) that was derived from that data set using the data-analysis method described in Sections 2.2.1 – 2.2.3. Consequently, the probability densities $P_{\text{org}}(x,t)$ and $P_{\text{rec}}(x,t)$ are normalized to unity like $\int_{-\infty}^{\infty} P_{\text{org}}(x,t)\,\mathrm{d}x = 1$ and $\int_{r_{\min}}^{r_{\max}} P_{\text{rec}}(x,t)\,\mathrm{d}x = 1$. In order to compare $P_{\text{org}}$ with $P_{\text{rec}}$ on the domain $[r_{\min}, r_{\max}]$ we first compute the re-normalization factor $M(t) = \int_{r_{\min}}^{r_{\max}} P_{\text{org}}(x,t)\,\mathrm{d}x < 1$ and subsequently compute the re-normalized distribution $P'_{\text{org}} = P_{\text{org}}/M(t)$. By definition, $P'_{\text{org}}$ is normalized to unity on the domain $[r_{\min}, r_{\max}]$ just as $P_{\text{rec}}$. Therefore, we can compare probability densities related to the original data and the reconstructed data on the basis of the distributions $P'_{\text{org}}$ and $P_{\text{rec}}$. Finally, we note that this test belongs to the class of self-consistency tests because in this test we first derive drift-diffusion models of the form (1) assuming that our a priori hypothesis is correct and subsequently assess the correctness of the hypothesis.

## 3 Examples

Let us illustrate explicitly how the proposed data-analysis technique can be applied to analyze noisy systems involving periodic drivers and time delays. To this end, we will use computer generated data. The first two examples will be concerned with data computed from two univariate benchmark models of time-delayed noisy systems with additive and parametric driving forces, see Section 3.1. In the last example we analyze computer generated data from a multivariate dynamical model that has been successfully applied to describe human tracking movements under time-delayed feedback control, see Section 3.2.

### 3.1 First order dynamical systems

#### 3.1.1 Additive sinusoidal driving force

The first example is an Ornstein-Uhlenbeck process subjected to a time-delayed feedback loop and an additive sinusoidal driver described by

$$\frac{\mathrm{d}}{\mathrm{d}t}X = \underbrace{-aX - bY + c\sin(\omega t)}_{h(X,Y,F(t))} + \sqrt{Q}\Gamma(t) \tag{17}$$

with $a, b, c > 0$. In equation (17) $\omega = 2\pi/T$ denotes the frequency of the driver and $Q$ describes the noise

[1] Note that in general we have $[r_{\min}, r_{\max}] \subset [x_{\min}, x_{\max}]$.

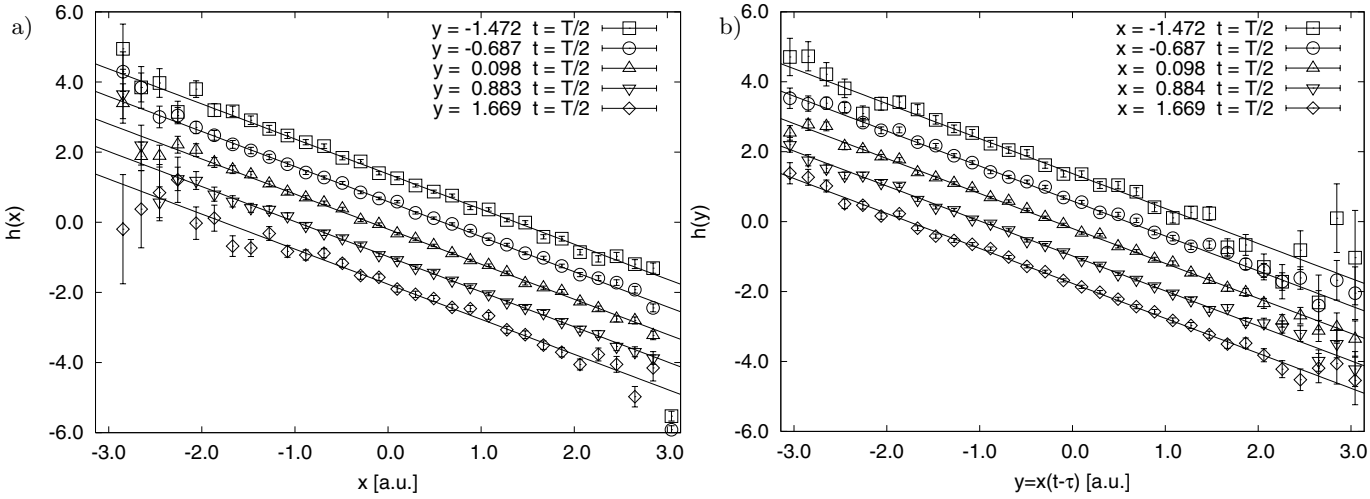


**Fig. 2.** Drift estimates $h$ for computer-generated data related to model (17) with additive driver and time-delayed feedback. Panel (a): $h$ versus $x$ for constant $t$ and several parameters $y$. Panel (b): $h$ versus $y$ for constant $t$ and several parameters $x$. Symbols represent estimates. Solid lines correspond to the original functions used to generate the data. Error bars correspond to one standard deviation of the estimates.

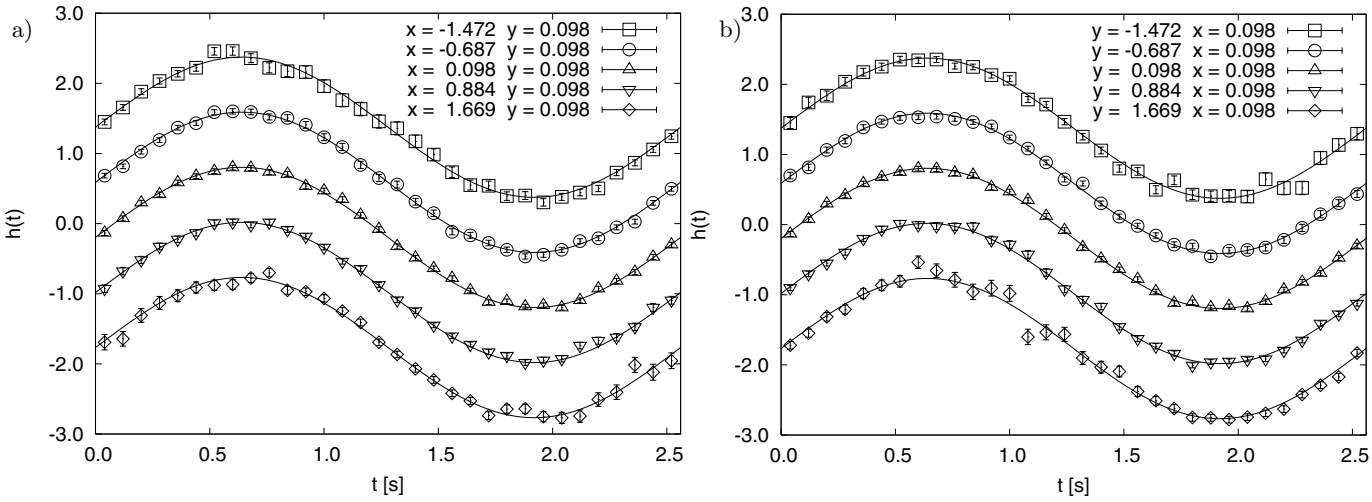


**Fig. 3.** Drift estimates $h$ for the model (17). Panel (a): $h$ versus $t$ for constant $y$ and several parameters $x$. Panel (b): $h$ versus $t$ for constant $x$ and several parameters $y$. Notations as in Figure 2.

amplitude. The time-delayed Ornstein-Uhlenbeck process without driving force (i.e. $c = 0$) has been investigated in several studies [83–88]. In this example the drift can be decomposed into three additive components

$$h(X, Y, F(t)) = h_x(X) + h_y(Y) + F(t) \qquad (18)$$

that reflect the impacts of a non-delayed restoring force $h_x$, the time-delayed feedback force $h_y$, and the periodic driving force $F$.

Using a modified Euler forward method [89], we generated a time series from the model (17) composed of $N$ data points $X_n$ (parameters $a = b = c = Q = 1$, $T = 2.56$, $\tau = 1$, $N = 10^9$, $\delta t = 0.01$).

We analyzed the computer generated data set on a domain $[x_{\min}, x_{\max}]$ with $x_{\min} = -\pi$ and $x_{\max} = \pi$. The phase space $\Omega(x, y, t) = [-\pi, \pi] \times [-\pi, \pi] \times [0, T]$ was divided into $32^3$ equidistant bins $\Delta\Omega_{ijk}$, see Section 2.2.3. That is, we had $\Delta x = \Delta y = 2\pi/32$ and $\Delta t = T/32$. In order to distinguish between the impacts of the forces $h_x$, $h_y$, and $F(t)$ we computed $h$ from equation (15). The reconstruction of $h$ is shown in Figures 2 and 3. Figure 2 shows $h$ as a function of $x$ for fixed values of $y$ and $t$ (panel (a)). In panel (b) the drift $h$ as a function of $y$ for fixed values of $x$ and $t$ is shown. That is, panel (a) reflects the behavior of $h_x(x)$, whereas panel (b) depicts the behavior of $h_y(y)$. Figure 3 shows $h$ as a function of $t$ for fixed values of $x$ and $y$. That is, Figure 3 primarily reveals the impact of $F(t)$. In Figures 2 and 3 both reconstructions of the drift $h$ based on equation (15) are shown and the corresponding original functions $h$. We see that the reconstructed functions are good approximations of the original ones. In general, the graphs shown in Figures 2 and 3 illustrate how the drift $h(x, y, t)$ looks like in terms of one-dimensional cuts through the three-dimensional phase space $\Omega$.

Assuming that we had no a priori knowledge about the underlying dynamical model, we could conclude on

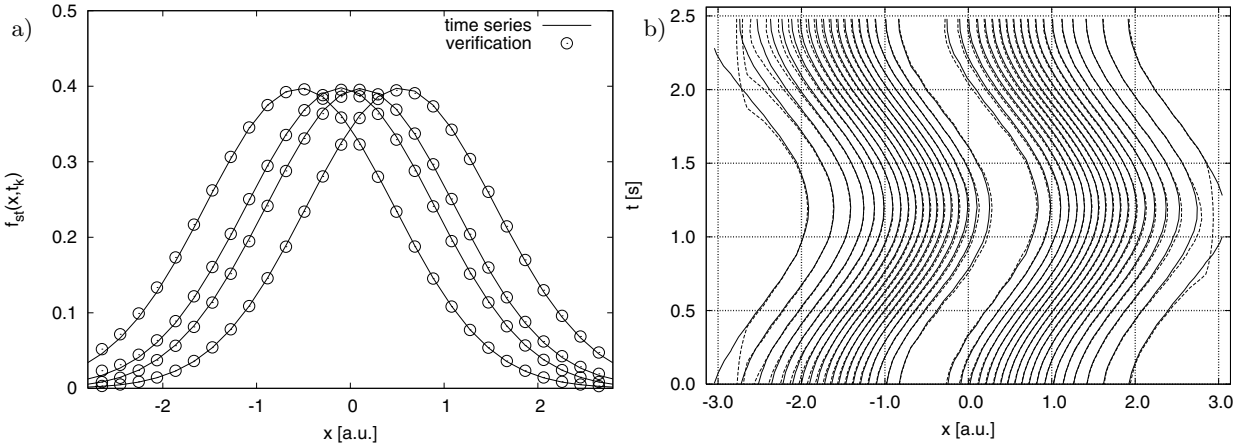


**Fig. 4.** Self-consistency test for the reconstruction of the model (17). Panel (a): reconstructed (symbols) and original (solid lines) probability densities $P_{\rm rec}$ and $P'_{\rm org}$ for several time points $t_k$. Panel (b): contour plot of the function $P_{\rm rec}(x,t)$ (solid lines) and $P'_{\rm org}(x,t)$ (dashed lines) in the $(x,t)$ plane. Each line represents a constant value $C$. That is, lines are defined by $C = P_{\rm rec}(x,t)$ and $C = P'_{\rm org}(x,t)$. $C$ values increase (decrease) in the left (right) part of the contour plot by $\Delta C$ ($\Delta C = 0.2$).

the basis of Figure 2b and Figure 3 that the dynamics involves a linear time-delayed feedback loop $h_y(y) = \lambda y$ and a periodic driving force $F(t) = A\sin(\omega t + \Phi)$. Moreover, we could determine the parameters $\lambda, A, \Phi$ from the graphs shown in Figure 2b and Figure 3 using, for example, regression analysis and least square fits [66,77,78,90,91].

The result of the self-consistency test (see Sect. 2.3) for the analyzed data set is shown in Figure 4. In the self-consistency test we neglected drift estimates that showed for fixed $t$ relatively large standard deviations (see error bars in Fig. 2, panels (a) and (b)). More precisely, the self-consistency test was performed on the domain $[r_{\min}, r_{\max}]$ with $r_{\min} = x_{\min} + \Delta x$ and $r_{\max} = x_{\max} - \Delta x$. In panel (a) of Figure 4 the probability densities $P'_{\rm org}$ and $P_{\rm rec}$ are shown for several time points $t$. We found that the reconstructed probability densities $P_{\rm rec}(x,t)$ were good approximations of the original probability density $P'_{\rm org}(x,t)$. In panel (b) of Figure 4 contour plots of $P'_{\rm org}(x,t)$ and $P_{\rm rec}(x,t)$ in the $(x,t)$ plane are shown. Again, $P_{\rm rec}(x,t)$ and $P'_{\rm org}(x,t)$ were almost identical.

### 3.1.2 Parametric sinusoidal driving force

In the next example we study a multiplicative coupling between the time-delayed coordinate and the driving force. That is, we have a parametric excitation of a time-delayed feedback loop. A fundamental model that can capture this kind of coupling reads

$$\frac{\mathrm{d}}{\mathrm{d}t}X = \underbrace{-aX + bY\sin(\omega t)}_{h(X,Y,F(t))} + \sqrt{Q}\,\Gamma(t) \qquad (19)$$

for $a, b, Q > 0$. Just as in the previous example, we first solved equation (19) numerically in order to generate a time series. The thus obtained time series contained $N$ data points $X_n$ (parameters $a = b = Q = 1$, $T = 2.56$, $\tau = 1$, $N = 10^9$, $\delta t = 0.01$).

The drift $h$ in the model (19) can be cast into the form

$$h(x, y, F(t)) = h_x(x) + h_y(y)F(t). \qquad (20)$$

In order to reveal this general structure and in particular to extract the multiplicative coupling $h_y(y)F(t)$ from the data set $\{X_1, \ldots, X_N\}$ we computed $h$ from equation (15). To this end we used the same phase space and the same phase space discretization as in the previous example. The result of our analysis is shown in Figures 5 and 6. Figure 5a shows the drift as a function of $x$ for fixed $y$ and $t$ and reflects the term $h_x(x)$. Figure 6b shows $h(x, y, F(t))$ as a function of $t$ for $x \approx 0$ and several values of $y$. From Figure 6b it is evident that the data set involves a time-dependent part $F(t)$ given by a sine function with the time-delayed coordinate $y$ as an amplitude. That is, Figure 6b shows the multiplicative interplay between the time-delayed feedback force and the periodic driving force. In Figure 6 the drift is plotted as a function of the time-delayed coordinate $y$ for fixed $t$ and $x$, respectively. In panel (a) the parameter $x$ is varied, whereas in panel (b) the parameter $t$ is varied. The drift $h(x, y, F(t))$ defined on the $(y, t)$ plane for fixed $x$ is shown in Figure 7. Panel (a) nicely illustrates the multiplicative nature of the coupling between the driver and the feedback. Panel (b) shows $h(x, y, F(t))$ for fixed $x$ in terms of a contour plot. In all panels of Figures 5 and 6 reconstructions of the drift $h$ based on equation (15) are shown as well as their corresponding original functions. We see that our data-analysis was able to reconstruct the original functions with a high degree of accuracy. In addition, the self-consistency test revealed that $P_{\rm rec}$ was virtually equivalent to $P'_{\rm org}$ on the scale shown in Figure 8.

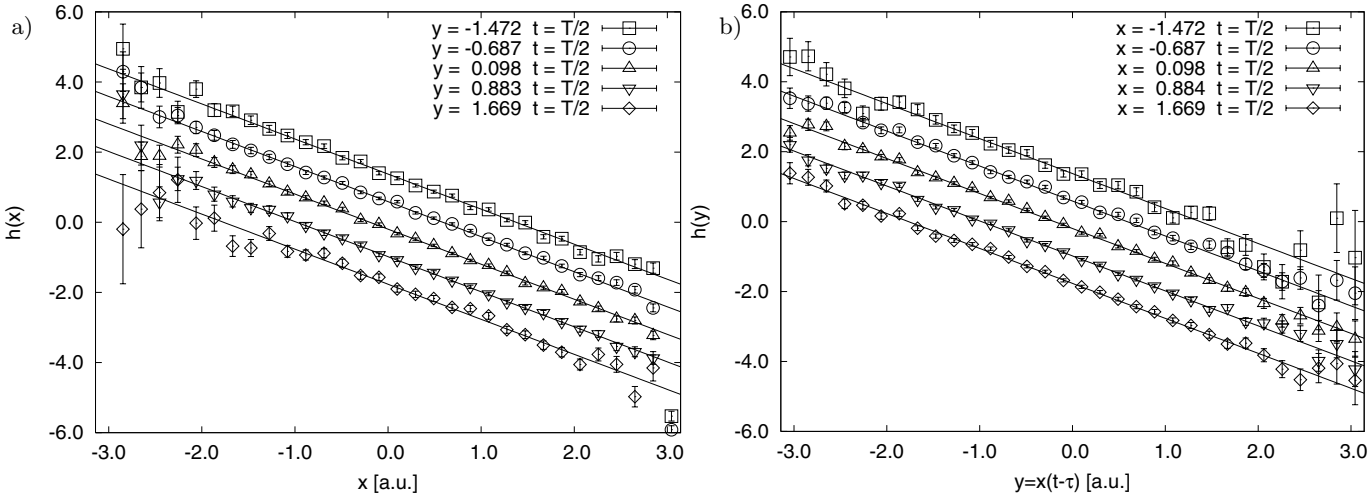


**Fig. 5.** Drift estimates $h$ for the model (19) with multiplicative coupling between driving force and time-delayed feedback force. Panel (a): $h$ versus $x$ for constant $t$ and several parameters $y$. Panel (b): $h$ versus $t$ for $x = 0.096$ and several parameters $y$. Notations as in Figure 2.

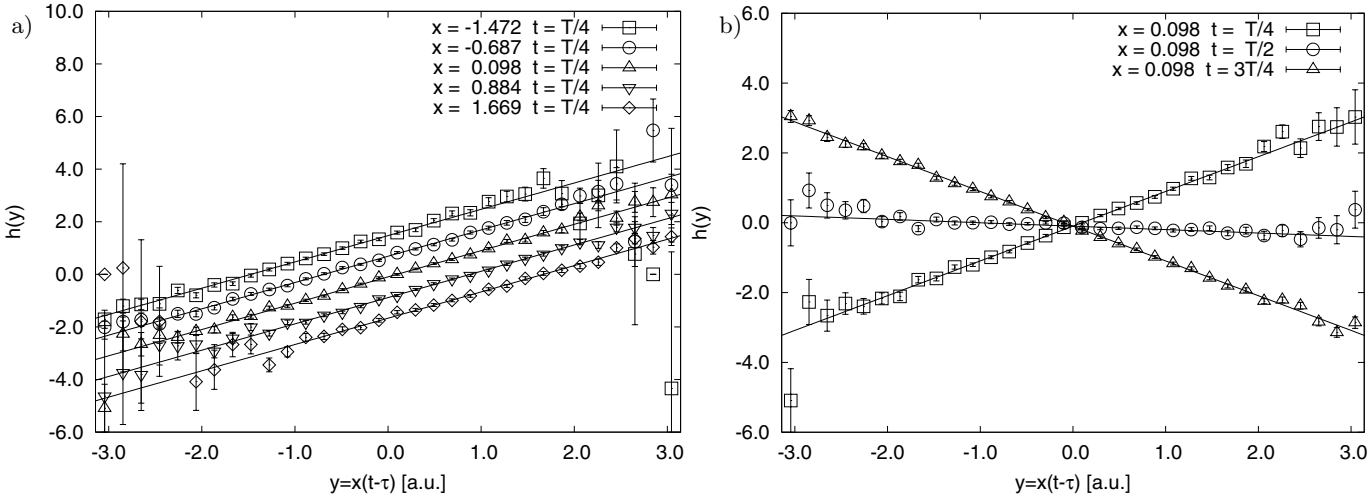


**Fig. 6.** Drift estimates $h$ for the model (19). Panel (a): $h$ versus $y$ for constant $t$ and several parameters $x$. Panel (b): $h$ versus $y$ for constant $x$ and several parameters $t$.

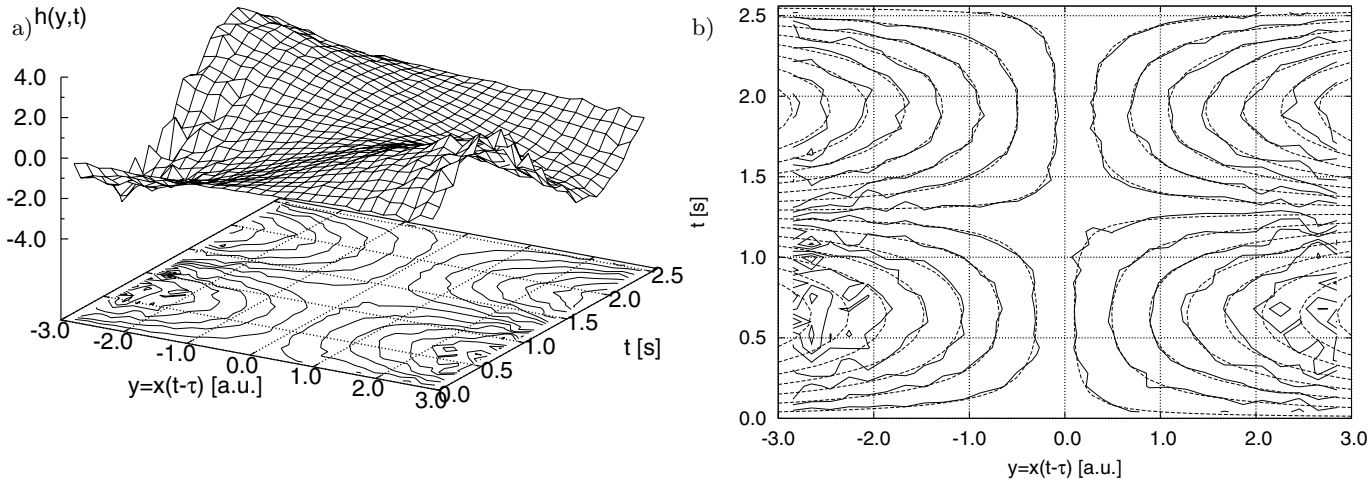


**Fig. 7.** Reconstruction of the drift $h$ in the $(y, t)$ plane for a fixed value of $x$ ($x = 0.098$). Panel (a): three-dimensional surface plot. Panel (b): contour plot with $\Delta C = 0.5$ (for notations see Fig. 4). Solid lines represent reconstruction estimates. Dashed lines correspond to the original function.

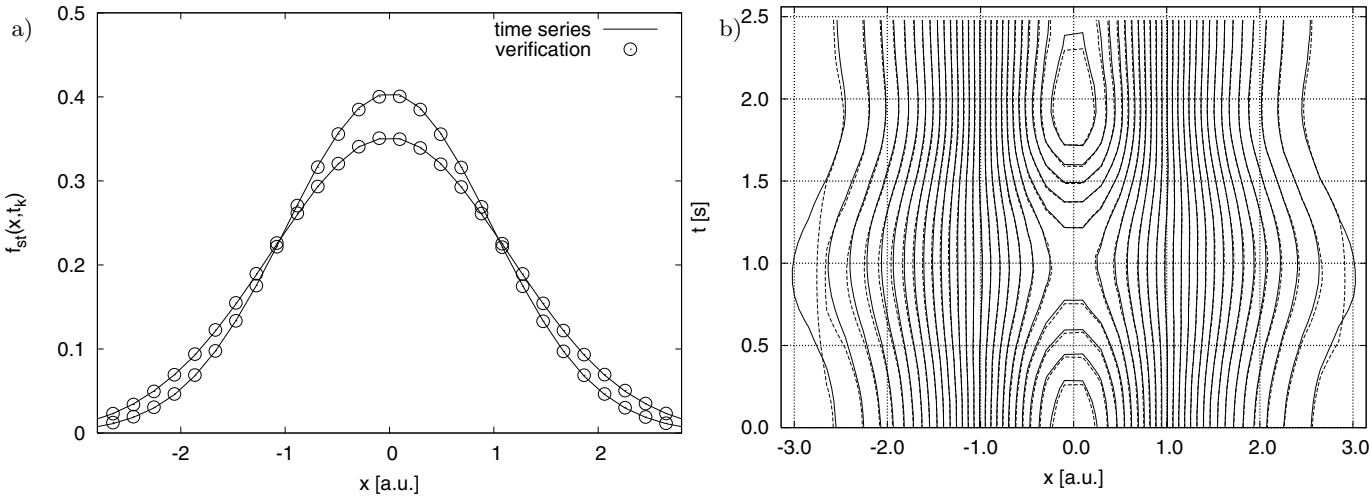


**Fig. 8.** Self-consistency test for data computed from the model (19). Panel (a): reconstructed (symbols) and original (solid lines) probability densities $P_{\rm rec}$ and $P'_{\rm org}$ for two different time points $t_k$. Panel (b): contour plots of $P_{\rm rec}(x,t)$ (solid lines) and $P'_{\rm org}(x,t)$ (dashed lines) in the $(x,t)$ plane ($\Delta C = 0.015$; for notations see Fig. 4).

### 3.2 Second-order dynamical systems and paced tapping

We now turn from first-order dynamical models of the form (2) to second-order dynamical models given by

$$\ddot{X} = h(X,\dot{X}) + u(Y,t) + \sqrt{Q}\Gamma(t). \tag{21}$$

In this context, we study data generated from a model that can be cast into the form (21). The model in question describes acoustically paced human tapping, that is, a particular class of coordinated movements. The study of coordinated movements in general has revealed many interesting insights into the organization of human motor control [48–51,92–95]. In addition, from a theoretical point of view it may be argued that the principles of nonlinear physics can be applied to motor control systems producing coordinated movements [2–4,96,97]. Therefore, coordinated movements in general and paced tapping in particular are of interest for movement scientists and physicists alike.

A sophisticated model describing the finger position $x$ during tapping reads [98]

$$\ddot{X} = a\dot{X} - \dot{X}^3 - \dot{X}X^2 - X + \beta\left[\sin(\omega t) - Y\right]^2 + \sqrt{Q}\,\Gamma(t) \tag{22}$$

with $a, \beta, Q > 0$. In the absence of a stimulus (i.e. for $\beta = 0$) the model describes self-paced tapping in terms of a nonlinear Van der Pol-Rayleigh oscillator. In the presence of a stimulus (i.e. for $\beta > 0$) the sine-term represents the impact of the periodic metronome beats. According to the tapping model (22), the motor control system compares the input stimulus $\sin(\omega t)$ with the time-delayed actual performance $Y(t) = X(t-\tau)$, where $\tau$ corresponds to the sensory delay of the system [98]. Finally, the additive fluctuating force with the noise amplitude $Q$ is assumed to describe perturbations arising due to neural background activity.

By means of the position and velocity variables $X$ and $V$, equation (22) can be equivalently expressed as

$$\dot{X} = V, \tag{23}$$

$$\dot{V} = \underbrace{V(a - X^2) - V^3 - X}_{h(x,v)} + \underbrace{\beta\left[\sin(\omega t) - Y\right]^2}_{u(y,t)} + \sqrt{Q}\,\Gamma(t). \tag{24}$$

By analogy to the data-analysis method discussed in Section 2.2.1 the drift term $h(x,y)+u(y,t)$ can be determined from a bivariate time-series $\{X(t_n), V(t_n), n = 1,\ldots,N\}$. To this end, a stroboscopic time averaging based on the velocity increments $V(t+\epsilon) - V(t)$ can be used in the following way:

$$h(x,v) + u(y,t_k) = \lim_{\epsilon\to 0} \frac{1}{\epsilon}\langle V(t_k+\epsilon) - v\rangle\Big|_{X(t_k)=x, X(t_k-\tau)=y, V(t_k)=v} \tag{25}$$

(see also Eq. (7)). As result one obtains the total drift term $h(x,y) + u(v,t)$. Due to the additional velocity variable the total drift term is defined on a four-dimensional phase space. This implies that in order to obtain accurate estimates for the drift term data sets are required that densely fill out this four-dimensional space, at least to a certain extent. That is, much more data points are required as in the case of the first-order dynamical models defined on three-dimensional phase spaces, see Section 3.1.

In what follows, we exploit our a priori knowledge that the total drift is composed of two components $h$ and $u$ that add up in an additive fashion $h_{\rm tot}(x,v,y,t) = h(x,v) + u(y,t)$. In line with previous studies [99,100] we will show next how the components $h(x,v)$ and $u(y,t)$ can be estimated separately using a two-step approach. It is clear that such a two-step approach requires fewer data points because the individual components $h(x,v)$ and

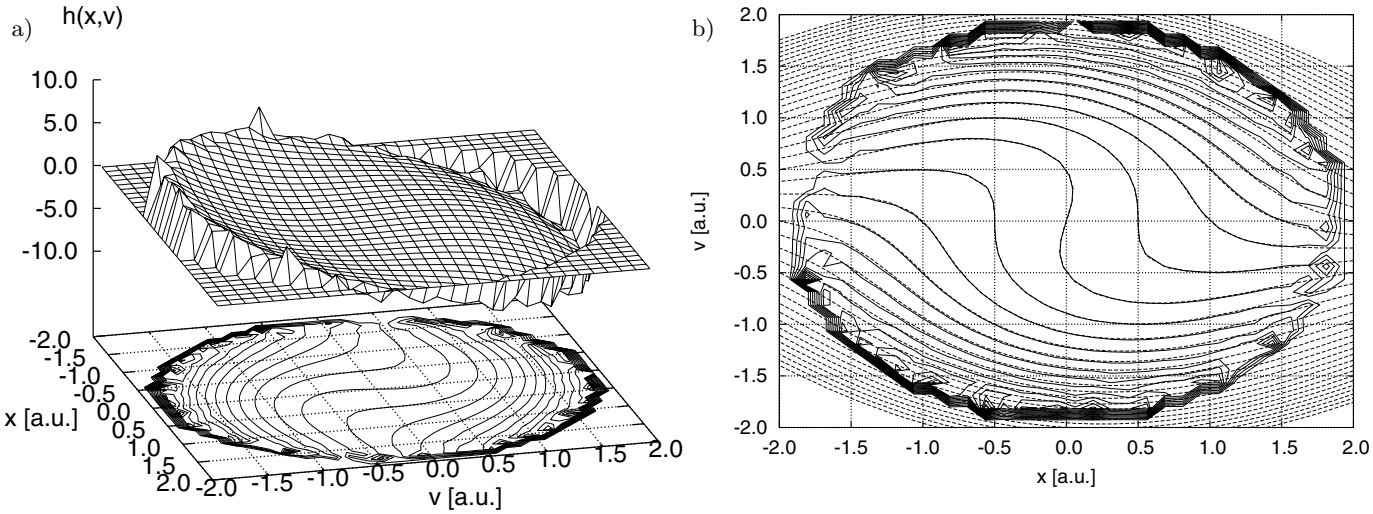


**Fig. 9.** Reconstruction of the drift component $h(x, v)$ of the second-order dynamical tapping model (24) in the $(x, v)$ plane. Panel (a): three-dimensional surface plot. Panel (b): contour plot with $\Delta C = 0.5$. Solid lines represent reconstruction estimates. Dashed lines correspond to the original function $h(x, v)$.

$u(y, t)$ are defined only on two-dimensional phase spaces. Let us elaborate on this two-step approach.

In the first step, a time series $\{X^a(t_n), V^a(t_n), n = 1, \ldots, N^a\}$ is evaluated that is recorded from the system defined by equation (21) in the absence of a feedback control and external driving. That is, in this case we have $u = 0$. In the context of human tapping, time series recordings of self-paced tapping ($\beta = 0$) have to be evaluated. From the velocity increments $V^a(t+\epsilon)-V^a(t)$ of such time series the drift term $h(x, v)$ can be computed like [61]

$$h(x,v) = \lim_{\epsilon \to 0} \frac{1}{\epsilon} \langle V^a(t+\epsilon) - v \rangle \Big|_{X^a(t)=x, V^a(t)=v} . \quad (26)$$

In this step the average represents time averaging. That is, neither a stroboscopic time averaging nor a constraint for the time-delayed position has to be introduced.

Having obtained $h(x, v)$, one can apply the data-analysis method to the entire driven feedback control system (21). That is, in a second step a time series $\{X^b(t_n), V^b(t_n), n = 1, \ldots, N^b\}$ recorded from the full system satisfying equation (21) with $u \neq 0$ is evaluated. With regard to our aforementioned motor control problem, this implies that acoustically paced tapping movements have to be examined. In this case we have $\beta > 0$ in the tapping model (22). Averaging equation (25) over $x$ and $v$ under the constraint $X^b(t_k - \tau) = y$, we then obtain

$$\langle h(x,v) \rangle|_{X^b(t_k-\tau)=y} + u(y,t_k) = \lim_{\epsilon \to 0} \frac{1}{\epsilon} \langle V^b(t_k+\epsilon) - v \rangle \Big|_{X^b(t_k-\tau)=y} . \quad (27)$$

That is, in the second step stroboscopic time averaging and the constraint $X(t_k - \tau) = y$ for the time-delayed variable are used. Recall that the function $h(x, v)$ has been determined in the first step of our analysis. Consequently, the expression $\langle h(x, v) \rangle|_{X^b(t_k-\tau)=y}$ can be derived from the time series $\{X^b(t_n), V^b(t_n), n = 1, \ldots, N^b\}$. Placing the term $\langle h(x, v) \rangle|_{X^b(t_k-\tau)=y}$ on the right hand side of equation (27), we obtain

$$u(y,t_k) = \lim_{\epsilon \to 0} \frac{1}{\epsilon} \langle V^b(t_k+\epsilon) - V^b(t_k) \rangle \Big|_{X^b(t_k-\tau)=y} - \langle h(x,v) \rangle|_{X^b(t_k-\tau)=y} . \quad (28)$$

To check whether the a priori assumption that the regarded system can be described by equation (21) is correct the self-consistency test discussed in Section 2.3 can be applied. The only difference to the examples studied in Section 3.1 is that one has to simulate a second-order differential equation as given in equation (21) or more specifically by equation (24) in order to compute $P_{\rm rec}$. Let us illustrate the two-step approach for computer generated data sets derived from the human tapping model (24).

We solved equation (24) numerically for $\beta = 0$ and $\beta = 0.4$ (other parameters: $a = 0.25$, $\tau = 0.4$, $T = 7.14$, $Q = 0.2$, $\delta t = 0.01$). In doing so, we generated two time series $[X^a(t_n), V^a(t_n)]$ with $n = 1, \ldots, N^a$ and $[X^b(t_n), V^b(t_n)]$ with $n = 1, \ldots, N^b$ ($N^a = N^b = 10^9$) representing self-paced and paced tapping, respectively. We computed $h(x, v)$ from $[X^a(t_n), V^a(t_n)]$ on a square domain $\Omega_a = [-2, 2] \times [-2, 2]$ using equation (26). To this end, $\Omega_a$ was discretized into $32^2$ bins with $\Delta x = 4/32$ and $\Delta v = 4/32$ and equation (26) was implemented on the computer just as discussed in Section 2.2.3 but with simple time averaging instead of stroboscopic time averaging (see discussion above). Subsequently, we estimated $u(y, t)$ from $[X^b(t_n), V^b(t_n)]$ on $\Omega_b = [-2, 2] \times [0, T]$ using equation (28). Again, we discretized $\Omega_b$ for that purpose into $32^2$ bins with $\Delta y = 4/32$ and $\Delta t = T/32$ and equation (28) was implemented on the computer as described in Section 2.2.3.

Figure 9 shows the result of our reconstruction of the drift component $h(x, v)$. The estimated component $h(x, v)$

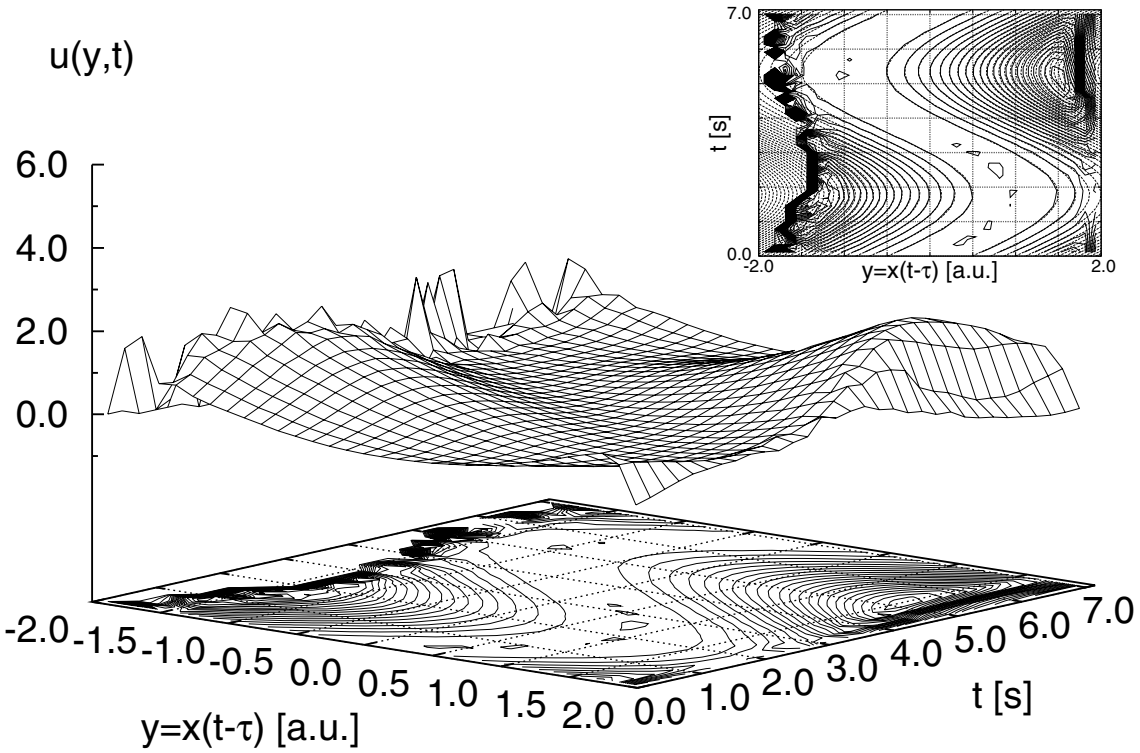


**Fig. 10.** Reconstruction of the drift component $u(y,t)$ of the model (24) in the $(y,t)$ plane (three-dimensional surface plot). Inlet: contour plot with $\Delta C = 0.5$.

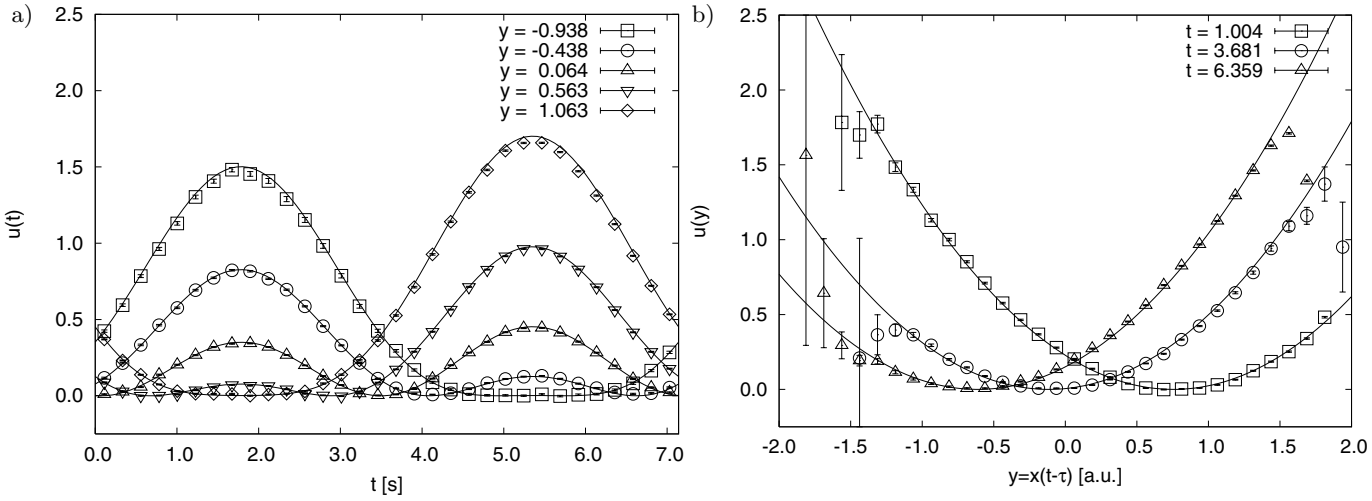


**Fig. 11.** Estimates for the drift component $u(y,t)$ of the tapping model (24). Panel (a): $u$ versus $t$ for several parameters $y$. Panel (b): $u$ versus $y$ for several parameters $t$. Notations as in Figure 2.

is plotted in the $(x,v)$ plane (panel (a)) and is shown as a contour plot (panel (b)). In addition, the original function $h(x,v)$ is shown as dashed lines in panel b of Figure 9. We found an excellent correspondence between the reconstruction and the original.

Figures 10 and 11 illustrate the reconstruction of the drift component $u(y,t)$ which contains information about the coupling between time-delayed feedback and driving force. In Figure 10 the reconstruction of $u(y,t)$ is shown in the full $(y,t)$ plane. In Figure 11 estimates of $u(y,t)$ are shown as functions of $t$ for fixed parameters $y$ (panel (a)) and as functions of $y$ for fixed values of $t$ (panel (b)). Comparing these estimates of $u(y,t)$ with the original functions, we found that in general the estimates were good approximations of the originals. However, for relatively large amplitudes of $y$ the standard deviation of the

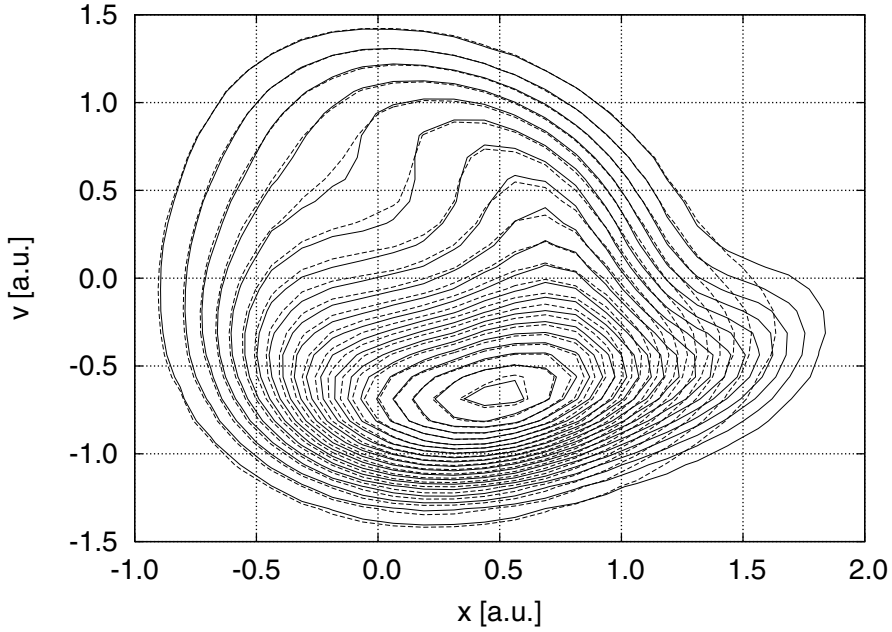


**Fig. 12.** Self-consistency test for computer generated data sets of the tapping model (24). Contour plots of the reconstructed (solid lines) and original (symbols) probability densities $\tilde{P}_{\rm rec}$ and $\tilde{P}_{\rm org}$ defined by equation (29) are shown in the $(x, v)$ plane ($\Delta C = 0.025/T$; for notations see Fig. 4).

estimates became large, see Figure 11b. Therefore, we defined the reconstructed model in the $(x, y)$ plane not on the domain $[-2, 2] \times [-2, 2]$ but on the slightly smaller domain $[r_{\min}, r_{\max}] \times [r_{\min}, r_{\max}]$ with $r_{\min} = -1.8$ and $r_{\max} = 1.8$.

The result of the self-consistency test is shown in Figure 12 in terms of a contour plot of $P'_{\rm org}$ and $P_{\rm rec}$ in the $(x, v)$ plane. Note that in contrast to the contour plot in Figure 4b that shows $P'_{\rm org}$ and $P_{\rm rec}$ in the $(x, t)$ plane, in Figure 12 we have eliminated the time variable $t$ by time averaging. That is, Figure 12 shows the function $\tilde{P}'_{\rm org}(x, v)$ and $\tilde{P}_{\rm rec}(x, v)$ defined by

$$\tilde{P}'_{\rm org}(x, v) = \frac{1}{T} \int_0^T P'_{\rm org}(x, v, t)\, {\rm d}t,$$
$$\tilde{P}_{\rm rec}(x, v) = \frac{1}{T} \int_0^T P_{\rm rec}(x, v, t)\, {\rm d}t. \qquad (29)$$

If the computer generated data sets $[X^a(t_n), V^a(t_n)]$ and $[X^b(t_n), V^b(t_n)]$ would correspond to experimental tapping recordings, the self-consistency test would indicate that the first-order statistical properties of the data sets can indeed be explained in terms of a non-autonomous stochastic delay differential equation model (21).

## 4 Conclusions

We showed how evolution equations of periodically driven systems with time-delayed feedback can be extracted from noisy data sets. On the basis of these evolution equations differential effects of the time-delayed feedback forces and the periodic driving forces can be identified. In doing so, our study bridged the gap between studies of periodically driven systems, on the one hand, and time-delayed systems, on the other.

By means of several computer generated data sets we illustrated explicitly how to apply the proposed data-analysis method. In all examples the reconstructions of the driving forces and the time-delayed feedback forces provided good approximations of the corresponding original functions. In the first example we were able to identify the additive interplay between the driving force and the feedback force, whereas in the second example we succeeded in identifying a multiplicative interplay between driver and feedback. In the final example related to paced tapping, we were able to identify the structure of the information-action coupling during paced tapping. More precisely, we identified a function $u$ that described how the action (time-delayed by the sensory delay) was coupled to the driving force. In sum, we demonstrated that differential effects due to driving, on the one hand, and feedback, on the other, can indeed be identified by the proposed data-analysis method.

For the analysis of second-order dynamical systems that can be cast into the form (21) a two-step approach was proposed. Using this approach, we were able to circumvent the data acquisition problem of how to fill a four-dimensional phase space with data points. Roughly speaking, the two-step approach replaced the

four-dimensional phase space by two two-dimensional phase spaces. Since in general time series analysis can better deal with two two-dimensional phase spaces than with one four-dimensional phase space, there is a clear advantage in applying the proposed two-step approach.

At several stages of our study we required some a priori knowledge about the data that we wanted to analyze. First of all, we assumed that the data can be described in terms of non-autonomous stochastic delay differential equations. Furthermore, we assumed that quantitative information about the relevant driving frequencies and the time delays is at our disposal. Indeed, some information concerning the magnitudes of time delays in biological systems is available in the literature (see e.g. [17,22,101]). Moreover, the time delays of technical applications can often be deduced from the construction plans of these applications. Finally, the driving frequencies are often well known from the context. In any case, the validity of a priori knowledge should be checked. To this end, we presented a self-consistency test based on first-order statistics. As stated in Section 2.3 higher-order statistics can be used for that purpose as well [58,82].

The data-analysis method presented in our study can be improved in many aspects. For example, adaptive bin sizes may be used instead of constant bin sizes in order to discretize the phase space of a system. More accurate estimates for the conditional changes of state variables such as $\dot{X}|_{X(t)=x}$ or $\dot{V}|_{V(t)=v}$ may be employed [78]. In this context not only higher-order approximation of conditional state changes may be used [78] but also the entire evolution of a state (i.e. its random path) may be evaluated [76]. Finally, the data-analysis method of the present study may be generalized in order to account for measurement noise that can have considerably different characteristic properties than dynamical noise [80,81].

## References


1. H. Haken, *Synergetics: Introduction and advanced topics* (Springer, Berlin, 2004)
2. J.A.S. Kelso, *Dynamic patterns — The self-organization of brain and behavior* (MIT Press, Cambridge, 1995)
3. H. Haken, *Principles of brain functioning* (Springer, Berlin, 1996)
4. V.K. Jirsa, J.A.S. Kelso, *Coordination dynamics: Issues and trends* (Springer, Berlin, 2004)
5. H. Risken, *The Fokker-Planck equation — Methods of solution and applications* (Springer, Berlin, 1989)
6. L. Gammaitoni, P. Hänggi, P. Jung, F. Marchesoni, Rev. Mod. Phys. **70**, 223 (1998)
7. P. Reimann, Phys. Rep. **361**, 57 (2002)
8. M.O. Magnasco, Phys. Rev. Lett. **71**, 1477 (1993)
9. H. Kamegawa, T. Hondou, F. Takagi, Phys. Rev. Lett. **80**, 5251 (1998)
10. N.S. Salas, A.C. Hernandez, Phys. Rev. E **68**, 046125 (2003)
11. D. Suzuki, T. Munakata, Phys. Rev. E **68**, 021906 (2003)
12. B.Q. Ai, X.J. Wang, G.T. Liu, D. Wen, H. Xie, W. Chen, L.G. Liu, Phys. Rev. E **68**, 061105 (2003)
13. L. Machura, M. Kostur, P. Talkner, J. Luczka, F. Marchesoni, P. Hänggi, Phys. Rev. E **94**, 233 (2004)
14. J.M. Cushing, *Integrodifferential equations and delay models in population dynamics* (Springer, Berlin, 1977)
15. M.C. Mackey, L. Glass, Science **197**, 287 (1977)
16. A. Longtin, J.G. Milton, J.E. Bos, M.C. Mackey, Phys. Rev. A **41**, 6992 (1990)
17. R.J. Peterka, J. Neurophysiol. **88**, 1097 (2001)
18. H. Haken, *Brain dynamics* (Springer, Berlin, 2002)
19. J.L. Cabrera, J.G. Milton, Phys. Rev. Lett. **89**, 158702 (2002)
20. A. Hutt, M. Bestehorn, T. Wennekers, Network Comp. in Neural Systems **14**, 351 (2003)
21. V.K. Jirsa, M. Ding, Phys. Rev. Lett. **93**, 070602 (2004)
22. A.V. Alexandrov, A.A. Frolov, F.B. Horak, P. Carlson-Kuhta, S. Park, Biol. Cybern. **93**, 309 (2005)
23. O.V. Popovych, C. Hauptmann, P.A. Tass, Phys. Rev. Lett. **94**, 164102 (2005)
24. S.F. Brandt, A. Pelster, R. Wessel, Phys. Rev. E **74**, 036201 (2006)
25. H.M. Gibbs, F.A. Hopf, D.L. Kaplan, R.L. Shoemaker, Phys. Rev. Lett. **46**, 474 (1981)
26. D. Lenstra, Opt. Commun. **81**, 209 (1991)
27. K. Pyragas, Phys. Lett. A **170**, 421 (1992)
28. I. Fischer, O. Hess, W. Elsäßer, E. Göbel, Phys. Rev. Lett. **73**, 2188 (1994)
29. B. Krauskopf, G.R. Gray, D. Lenstra, Phys. Rev. E **58**, 7190 (1998)
30. M. Bestehorn, E.V. Grigorieva, H. Haken, S.A. Kaschenko, Physica D **145**, 110 (2000)
31. L.S. Tsimring, A. Pikovsky, Phys. Rev. Lett. **87**, 250602 (2001)
32. C. Masoller, Phys. Rev. Lett. **88**, 034102 (2002)
33. J. Schlesner, A. Amann, N.B. Janson, W. Just, E. Schöll, Phys. Rev. E **68**, 066208 (2003)
34. M. Schanz, A. Pelster, Phys. Rev. E **67**, 056205 (2003)
35. N.B. Janson, A.G. Balanov, E. Schöll, Phys. Rev. Lett. **93**, 010601 (2004)
36. T. Erneux, L. Lager, M.W. Lee, J. Goedgebuer, Physica D **194**, 49 (2004)
37. K.U. Smith, *Delayed sensory feedback and behavior* (W. B. Saunders Company, Philadelphia, 1962)
38. G. Stepan, *Retarded dynamical systems: Stability and characteristic functions* (Longman Scientific & Technical, New York, 1989)
39. W. Wischert, A. Wunderlin, A. Pelster, M. Olivier, J. Groslambert, Phys. Rev. E **49**, 203 (1994)
40. A. Namajunas, K. Pyragas, A. Tamasevicius, Phys. Lett. A **201**, 42 (1995)
41. H.A. Braun, R.A. Henning, in *Meeting of the American Society of Ergonomics Systems Engineering,* Sept. 13–14, Madison, Wisconsin, 1996
42. C. Simmendinger, A. Wunderlin, A. Pelster, Phys. Rev. E **59**, 5344 (1999)
43. G. Radons, R. Neugebauer, *Nonlinear dynamics of production systems* (Wiley-VCH, Berlin, 2004)
44. K. Patanarapeelert, T.D. Frank, P.J. Beek, R. Friedrich, I.M. Tang, Phys. Rev. E **73**, 021901 (2006)
45. D. Wu, S. Zhu, Phys. Rev. E **73**, 051107 (2006)
46. T. Schreiber, Phys. Rep. **308**, 1 (1999)
47. H. Kantz, T. Schreiber, *Nonlinear time series analysis* (Cambridge University Press, Cambridge, 1997)

48. J.A.S. Kelso, Am. J. Physiol. Regul. Integr. Comp. Physiol. **15**, R1000 (1984)
49. H. Haken, J.A.S. Kelso, H. Bunz, Biol. Cybern. **51**, 347 (1985)
50. P.J. Beek, W.E.I. Rikkert, P.C.W. van Wieringen, J. Exp. Psychol. - Hum. Percept. Perform. **22**, 1077 (1996)
51. P. Tass, J. Kurths, M.G. Rosenblum, G. Guasti, H. Hefter, Phys. Rev. E **54**, R2224 (1996)
52. U. Langenberg, H. Hefter, K.R. Kessler, J.D. Crooke, Exp. Brain Res. **118**, 161 (1998)
53. A. Daffertshofer, C. van den Berg, P.J. Beek, Physica D **132**, 243 (1999)
54. C. van den Berg, P.J. Beek, R.C. Wagenaar, P.C.W. van Wieringen, Exp. Brain Res. **134**, 174 (2000)
55. T.D. Frank, P.J. Beek, R. Friedrich, Phys. Lett. A **338**, 74 (2005)
56. R.D. Driver, *Ordinary and delay differential equations — Applied mathematical sciences* (Springer, New York, 1977), Vol. 20
57. R.C. Dorf, R.H. Bishop, *Modern control systems* (Addison Wesley, Reading MA, 1995)
58. R. Friedrich, J. Peinke, Phys. Rev. Lett. **78**, 863 (1997)
59. R. Friedrich, J. Peinke, C. Renner, Phys. Rev. Lett. **84**, 5224 (2000)
60. R. Friedrich, S. Siegert, J. Peinke, S. Lück, M. Seifert, M. Lindemann, J. Raethjen, G. Deuschl, G. Pfister, Phys. Lett. A **271**, 217 (2000)
61. J. Gradisek, S. Siegert, R. Friedrich, I. Grabec, Phys. Rev. E **62**, 3146 (2000)
62. G.R. Jafari, S.M. Fazeli, F. Ghasemi, S.M.V. Allaei, M.R.R. Tabar, A.I. Zad, G. Kavei, Phys. Rev. Lett. **91**, 226101 (2002)
63. T. Kuusela, Phys. Rev. E **69**, 031916 (2004)
64. M. Waechter, F. Riess, T. Schimmel, U. Wendt, J. Peinke, Eur. Phys. J. B **41**, 259 (2004)
65. A.M. van Mourik, A. Daffertshofer, P.J. Beek, Phys. Lett. A **351**, 13 (2006)
66. A.M. van Mourik, A. Daffertshofer, P.J. Beek, Biol. Cybern. **94**, 233 (2006)
67. J. Gradisek, R. Friedrich, E. Govekar, I. Grabec, Phys. Lett. A **294**, 234 (2002)
68. T.D. Frank, P.J. Beek, R. Friedrich, Phys. Lett. A **328**, 219 (2004)
69. M.J. Bünner, T. Meyer, A. Kittel, J. Parisi, Phys. Rev. E **56**, 5083 (1997)
70. R. Hegger, M.J. Bünner, H. Kantz, Rev. Phys. Lett. **81**, 558 (1998)
71. V.I. Ponomarenko, M.D. Prokhorov, Phys. Rev. E **66**, 026215 (2002)
72. K. Ito, Proc. Imperial Acad. Tokyo **20**, 519 (1944)
73. S.A. Mohammed, *Stochastic analysis and related topics VI*, edited by I. Decreusefond, J. Gjerde, B. Oksendal, A.S. Üstünel (Birkhäuser, Boston, 1998), pp. 1–77
74. T.D. Frank, Phys. Rev. E **71**, 031106 (2005)
75. R.L. Stratonovich, *Topics in the theory of random noise* (Gordon and Beach, New York, 1963), Vol. 1
76. D. Kleinhans, R. Friedrich, A. Nawroth, J. Peinke, Phys. Lett. A **346**, 42 (2005)
77. T.D. Frank, M. Sondermann, T. Ackemann, R. Friedrich, Nonlin. Phenom. Complex Syst. **8**, 193 (2005)
78. K. Patanarapeelert, T.D. Frank, R. Friedrich, P.J. Beek, I.M. Tang, Phys. Lett. A **360**, 190 (2006)
79. P. Sura, J. Barsugli, Phys. Lett. A **305**, 304 (2002)
80. M. Siefert, A. Kittel, R. Friedrich, J. Peinke, Europhys. Lett. **61**, 466 (2003)
81. F. Böttcher, J. Peinke, D. Kleinhans, R. Friedrich, P.G. Lind, M. Haase, Phys. Rev. Lett. **97**, 090603 (2006)
82. C. Renner, J. Peinke, R. Friedrich, Physica A **298**, 499 (2001)
83. T.D. Frank, P.J. Beek, R. Friedrich, Phys. Rev. E **68**, 021912 (2003)
84. U. Küchler, B. Mensch, Stoch. Stoch. Rep. **40**, 23 (1992)
85. M.C. Mackey, I.G. Nechaeva, Phys. Rev. E **52**, 3366 (1995)
86. S. Guillouzic, I. L' Heureux, A. Longtin, Phys. Rev. E **59**, 3970 (1999)
87. A.A. Budini, M.O. Caceres, Phys. Rev. E **70**, 046104 (2004)
88. A. Amann, E. Schöll, W. Just, Physica A **373**, 191 (2007)
89. K. Patanarapeelert, T.D. Frank, R. Friedrich, I.M. Tang, J. Phys. A **38**, 10069 (2005)
90. H.U. Bödeker, M.C. Röttger, A. Liehr, T.D. Frank, R. Friedrich, H.G. Purwins, Phys. Rev. E **67**, 056220 (2003)
91. T.D. Frank, R. Friedrich, P.J. Beek, Phys. Rev. E **74**, 051905 (2006)
92. D. Sternad, M.T. Turvey, R.C. Schmidt, Biol. Cybern. **67**, 223 (1992)
93. C.E. Peper, P.J. Beek, P.C.W. van Wieringen, J. Exp. Psychol. - Hum. Percept. Perform. **21**, 1117 (1995)
94. E.L. Amazeen, P.G. Amazeen, P.J. Treffner, M.T. Turvey, J. Exp. Psychol. - Hum. Percept. Perform. **23**, 1552 (1997)
95. F. Mechsner, D. Kerzel, G. Knoblich, W. Prinz, Nature **414**, 69 (2001)
96. M.T. Turvey, Am. Psychol. **45**, 938 (1990)
97. P.J. Beek, C.E. Peper, D.F. Stegeman, Hum. Mov. Sci. **14**, 573 (1995)
98. Y. Chen, M. Ding, J.A.S. Kelso, Phys. Rev. Lett. **79**, 4501 (1997)
99. H.U. Bödeker, A. Liehr, M.C. Röttger, T.D. Frank, R. Friedrich, H.G. Purwins, New J. Phys. **6**, 62 (2004)
100. T.D. Frank, R. Friedrich, P.J. Beek, Stoch. Dyn. **5**, 297 (2005)
101. J. Gross, P.A. Tass, S. Salenius, R. Hari, H.J. Freund, A. Schnitzler, J. Physiology **527**, 623 (2000)